Discontinuous Galerkin Time-Domain solution of Maxwell's equations on locally-refined grids with fictitious domains

A. Bouquet,
INRIA Sophia Antipolis and France Telecom R&D, La Turbie, France,

C. Dedeban,
France Telecom R&D, La Turbie, France,

S. Piperno,
CERMICS, Université Paris-Est, Marne-la-Vallée, France

Keywords Time-domain Discontinuous Galerkin methods, locally-refined grids, fictitious domain approach, energy conservation, centered fluxes

Abstract
The use of the prominent FDTD method for the time-domain scattering of electromagnetic waves by devices with small geometrical details can require very fine grids and lead to unmanageable computational time and storage. We propose an extension of a Discontinuous Galerkin Time-Domain (DGTD) method to locally-refined, possibly non-conforming meshes, coupled to a fictitious domain approach. The DGTD method we use is set on block-structured grids of orthogonal elements and is based on centered flux approximations for surface integrals and a second-order leap-frog scheme for advancing in time. The stability of the method has been analyzed previously, it is proved that a discrete electromagnetic energy is exactly preserved. The dispersion analysis is completed in this paper. Also, new features of the method are introduced herein: the use of PML regions in a DG context has been detailed, and a first step towards the coupling with a fictitious domain approach has been done, leading to very promising preliminary numerical results.

Structured Abstract
Research paper

Purpose. The use of the prominent FDTD method for the time-domain solution of electromagnetic wave propagation past devices with small geometrical details can require very fine grids and can lead to unmanageable computational time and storage. We extend the analysis of a DGTD method (able to handle possibly non-conforming locally refined grids, based on portions of Cartesian grids) and investigate the use of PML regions and the coupling with a fictitious domain approach.
Design/methodology/approach. Based on a Discontinuous Galerkin Time-Domain method, we develop a fictitious domain approach to deal with complex and small geometrical details.
Findings. The fictitious domain approach is a very interesting complement to the FDTD method, since it makes possible to handle complex geometries. However, the fictitious domain approach requires small volumic elements, thus making the use of the FDTD on wide, regular, fine grids often unmanageable. The DGTD method has the ability to handle easily locally-refined grids and we show it can be coupled to a fictitious domain approach.
Research limitations/implications. Although the stability and dispersion analysis of the DGTD method is complete, the theoretical analysis of the fictitious domain approach in the DGTD context is not. It is a subject of further investigation (which could provide important insights for potential improvements).
Originality/value. To our knowledge, it is the first time a DGTD method is coupled with a fictitious domain approach.

1 Introduction

The solution of the time-domain Maxwell equations on space grids is nowadays commonly used for the modeling of systems involving electromagnetic waves. Although the Finite Difference Time-Domain (FDTD) methods based on Yee's scheme [36] are still prominent, the urge for handling complex structures and complex geometries has motivated the proposition of several methods able to deal with unstructured meshes, like Finite Element Time-Domain (FETD) methods [24, 26], Finite Volume Time-Domain (FVTD) methods [9, 22] and Discontinuous Galerkin Time-Domain methods [10], meeting a tremendous development in particular because they can lead to high orders of accuracy by simply choosing suitable basis functions [20, 29], either based on upwind or partially upwind fluxes with multi-step low-storage Runge-Kutta time-schemes [20] (leading to slightly diffusive approximations) or on centered fluxes and leap-frog time schemes [30], leading to slightly less accurate but energy preserving approximations.

Although increasing numbers of numerical simulations of electromagnetic and electronic systems are being made on unstructured (mostly tetrahedral) grids rather than Cartesian grids and using DGTD methods rather FDTD methods, computations on structured grids are in general easier to prepare and post-process, in particular because of the existence of pre- and post-processing tools initially developed for FDTD methods. Therefore, the investigation of accurate and efficient DGTD methods on Cartesian grids is still a question of interest [2]. However, Cartesian grids are not adapted to complex geometries. In the presence of complex structures, two solutions were imagined in the restricted context of FDTD methods, and each of these solutions can be re-examined in the context of DGTD methods:

- use locally refined (conforming or non-conforming) cartesian grids and replace the complex boundary of structures by an approximate staircased boundary: artificial scatterings lead in that case to limited inaccuracies [7] if the grid is refined; whenever the mesh is locally refined, it is well known that FDTD couplings generally show long time instabilities [25, 31]; in the context of DGTD method, the use of non-conforming block-Cartesian grids has already been proposed [8], with proved stability and accuracy, but the treatment of staircased artificial boundaries could also pollute the solutions.

- use a fictitious domain approach, where the boundary condition on the physical boundary is handled in a least-square sense via a projection on a discrete constraint; this method, introduced in the 1960's for elliptic problems, was applied to numerous domains [3, 17, 35], including time-domain wave propagations problems [11, 15]; the main part of the computational time is devoted to computations on the volumic Cartesian grid, a small part being devoted to the computation of Lagrange multipliers corresponding to the constraint on the object boundary.

In general, the fictitious domain approach can produce an approximate solution of Maxwell equations only if some compatibility condition is satisfied between the element size of the surfacic mesh of the object and size of volumic elements [35, 3]. Therefore, a small geometrical detail on the surface of the object, leading to small surfacic elements, leads necessarily to locally small volumic elements, and the global computation can be done only if a locally-refined volumic grid can be dealt with. This sums up the aim of this paper: to build a fictitious domain approach based on DGTD method and to produce preliminary numerical results on complex geometries with locally refined meshes, the DGTD implementation of UPML regions [37] being an additional feature.

The paper is organized as follows: in Section 2, the general framework of DGTD methods considered is introduced, as well as the particular choice of brick elements and local approximation spaces; in Section 3, the UPML medium used is presented, along with the implementation of the DG space-discretization; Section 4 is devoted to the fictitious domain approach proposed; preliminary numerical results are presented in Section 5 and conclusions and further investigations are drawn in Section 6.

2 DG methods for time-domain electromagnetics

We consider the three-dimensional time-domain Maxwell's equations for heterogeneous anisotropic linear media with source $\vec{\mathbf{j}}$ (current density). The electric permittivity tensor $\bar{\bar{\varepsilon}}(x)$ and the magnetic

permeability tensor $\bar{\bar{\mu}}(x)$ are symmetric positive definite, varying in space and uniformly bounded. The electromagnetic field $(\vec{E}, \vec{H})$ verify the following Maxwell equations, where divergence constraints have been dropped:

$$\begin{cases} \bar{\bar{\varepsilon}} \dfrac{\partial \vec{E}}{\partial t} = \vec{\text{curl}}\, \vec{H} - \vec{\mathbf{j}}, \\ \bar{\bar{\mu}} \dfrac{\partial \vec{H}}{\partial t} = -\vec{\text{curl}}\, \vec{E}. \end{cases} \tag{1}$$

Replacing in the equations above the $\vec{\text{curl}}$ operator by three directional partial derivatives of fluxes, Maxwell equations can be rewritten as a set of balance equations in conservative form.

We mainly consider exterior problems with metallic objects (volumes or surfaces). The problem can be set on a bounded domain Ω of $\mathbb{R}^3$, with an exterior metallic boundary condition (*i.e.* $\vec{n} \times \vec{E} = \vec{0}$) or an absorbing boundary condition (Silver-Müller first-order condition $\vec{n} \times \vec{E} = -c\mu\ \vec{n} \times (\vec{n} \times \vec{H})$ or PML-type) on the exterior boundary $\partial\Omega_\infty$ (here, $\vec{\tilde{n}}$ denotes the unitary outwards normal).

2.1 General principle of DG methods

The general principle of DG methods, used for the solution of Partial Differential Equations in conservative form consists in 1) using a partition of the computational domain into polyhedra (called cells or elements); 2) for each cell, choosing a local set of basis fields and assume the fields will be approximated by linear combinations of these fields; hence, the approximate fields will be *a priori* discontinuous at element faces; 3) use an element-base integral form of the equations at hand and, after integrating by parts, handle numerically all surface integrals on element faces, for which the approximate field is discontinuous. The reader can refer to a rich literature on the subject, in particular in electromagnetics [8, 14, 20].

The Discontinuous Galerkin approach has many advantages, like easy implementation, in particular in a parallel computation setting, easy use of so-called *hp*-refinement (variable size and order of accuracy through elements), possible use of non-conforming meshes. The most simple DG method at hand consists in approximating fields by constants inside elements, which yields a simple finite volume approximation. The reader can find a detailed description on the method on unstructured tetrahedral meshes in [14] as well as on locally-refined block cartesian grids [8].

In the most general case, for each polyhedral element $\mathcal{T}_i$, the local electric permittivity tensor $\bar{\bar{\varepsilon}}_i$ and the local magnetic permeability tensor $\bar{\bar{\mu}}_i$ are assumed constant inside the element $\mathcal{T}_i$. We call interface between two neighboring elements their intersection (if it is a surface with nonzero two-dimensional measure). One should notice that this interface can be only a part of a face of one hexahedron in a non-conforming case. For each internal interface $a_{ik} = \mathcal{T}_i \bigcap \mathcal{T}_k$, we denote by $\vec{n}_{ik}$ the integral over the interface of the unitary normal, oriented from $\mathcal{T}_i$ towards $\mathcal{T}_k$ (same definitions are extended to boundary interfaces, the index k corresponding to a ghost element outside the domain). We denote by $\vec{\tilde{n}}_{ik} = \vec{n}_{ik}/\|\vec{n}_{ik}\| = {}^t(\tilde{n}_{ikx}, \tilde{n}_{iky}, \tilde{n}_{ikz})$ the normalized normals and by $\mathcal{V}_i$ the set of elements neighboring $\mathcal{T}_i$ (i.e. having an interface in common with $\mathcal{T}_i$). Inside each element $\mathcal{T}_i$, the approximated fields $\vec{\mathbf{E}}_i(x,t)$ and $\vec{\mathbf{H}}_i(x,t)$ are searched for as linear combinations of chosen local basis of vector fields $\vec{\varphi}_{ij}, 1 \leq j \leq d_i$, where d_i denotes the local number of scalar degrees of freedom, *i.e.* for example, $\forall x$ in $\mathcal{T}_i$, $\vec{\mathbf{E}}_i(x,t) = \sum_{1 \leq j \leq d_i} E_{ij}(t)\ \vec{\varphi}_{ij}(x)$. Dot-multiplying (1) by a given basis function $\vec{\varphi}_{ij}$, integrating over $\mathcal{T}_i$ and integrating by parts, yields 1) well-defined volume integrals and 2) surface integrals for which an approximation has to be made (in order to compute values at the boundaries of the element). In the particular context of linear time-domain wave propagation problems, one can use totally centered fluxes (*i.e.* the approximate values for electromagnetic fields at $a_{ik} = \mathcal{T}_i \bigcap \mathcal{T}_k$ are simply the average values of traces on both sides) coupled with a leap-frog time-discretization scheme with a given time-step Δt (in the sequel, superscripts refer to time-stations; unknowns related to the electric (resp. magnetic) field are approximated at integer (resp. half-integer) time-stations). Thus, (1) is discretized in time and space

as

$$\left\{ \begin{array}{l} \left(M_i^{\epsilon} \ \dfrac{\vec{\mathbf{E}}_i^{n+1} - \vec{\mathbf{E}}_i^{n}}{\Delta t} \right)_j = \displaystyle\int_{\mathcal{T}_i} \vec{\mathrm{curl}}\, \vec{\varphi}_{ij}.\vec{\mathbf{H}}_i^{n+1/2} - \int_{\mathcal{T}_i} \vec{\mathbf{j}}^{n+1/2}.\vec{\varphi}_{ij} - \displaystyle\sum_{k\in\mathcal{V}_i} \int_{a_{ik}} (\vec{\varphi}_{ij} \times \frac{\vec{\mathbf{H}}_i^{n+1/2} + \vec{\mathbf{H}}_k^{n+1/2}}{2}).\vec{\vec{n}}_{ik} \ , \\ \left(M_i^{\mu} \ \dfrac{\vec{\mathbf{H}}_i^{n+3/2} - \vec{\mathbf{H}}_i^{n+1/2}}{\Delta t} \right)_j = - \displaystyle\int_{\mathcal{T}_i} \vec{\mathrm{curl}}\, \vec{\varphi}_{ij}.\vec{\mathbf{E}}_i^{n+1} + \sum_{k\in\mathcal{V}_i} \int_{a_{ik}} (\vec{\varphi}_{ij} \times \frac{\vec{\mathbf{E}}_i^{n+1} + \vec{\mathbf{E}}_k^{n+1}}{2}).\vec{\vec{n}}_{ik} \ . \end{array} \right. \tag{2}$$

where the j subscripts denote the jth component of vectors in the left hand side, $\vec{\mathbf{E}}_i$ and $\vec{\mathbf{H}}_i$ denote the column vectors of scalar degrees of freedom inside elements, and M_i^{ϵ} and M_i^{μ} are local square (symmetric positive definite) mass matrices of size d_i, with general terms $(M_i^{\epsilon})_{jl} = \int_{\mathcal{T}_i} {}^t\vec{\varphi}_{ij}\bar{\bar{\varepsilon}}_i\vec{\varphi}_{il}$, $(M_i^{\mu})_{jl} = \int_{\mathcal{T}_i} {}^t\vec{\varphi}_{ij}\bar{\bar{\mu}}_i\vec{\varphi}_{il}$.

The time and space discretization proposed leads to a quasi-explicit, energy-conserving (in the absence of absorbing boundaries), dissipation-free numerical method and a stability result exists in the general case of arbitrary polyhedral grids [14], with a CFL-like stability condition on Δt. Convergence is proved at least in cases where the physical medium has piecewise constant properties [10, 14].

2.2 A particular DGTD method on orthogonal hexahedra

In his PhD thesis, N. Canouet proposed to use particular DGTD methods, adapted to block-cartesian grids [8]. Two methods were indeed considered, each deriving from the scheme (2) with a particular choice for the sets of local fields $\vec{\varphi}_{ij}$. For each hexahedron $\mathcal{T}_i$, let us introduce $\mathbf{G_i} = {}^t(x_{Gi}, y_{Gi}, z_{Gi})$ its mass center and $\mathbf{\Delta} = {}^t(\Delta x_i, \Delta y_i, \Delta z_i)$ its sizes. The two DG finite element spaces are:

- the **DG**-$\mathbb{P}^1_{div}$ method, deriving from the 9 following L^2-orthogonal basis functions:

$$\left\{ \begin{array}{lll} \vec{\varphi}_{i1} = {}^t(1,0,0), & \vec{\varphi}_{i2} = {}^t(y - y_{Gi}, 0, 0), & \vec{\varphi}_{i3} = {}^t(z - z_{Gi}, 0, 0), \\ \vec{\varphi}_{i4} = {}^t(0,1,0), & \vec{\varphi}_{i5} = {}^t(0, x - x_{Gi}, 0), & \vec{\varphi}_{i6} = {}^t(0, z - z_{Gi}, 0), \\ \vec{\varphi}_{i7} = {}^t(0,0,1), & \vec{\varphi}_{i8} = {}^t(0, 0, x - x_{Gi}), & \vec{\varphi}_{i9} = {}^t(0, 0, y - y_{Gi}). \end{array} \right. \tag{3}$$

- the **DG**-$\mathbb{Q}^1_{div}$ method, deriving from the functions (3) completed by

$$\left\{ \begin{array}{l} \vec{\varphi}_{i10} = {}^t((y - y_{Gi})(z - z_{Gi}), 0, 0), \\ \vec{\varphi}_{i11} = {}^t(0, (x - x_{Gi})(z - z_{Gi}), 0), \\ \vec{\varphi}_{i12} = {}^t(0, 0, (x - x_{Gi})(y - y_{Gi})). \end{array} \right. \tag{4}$$

Since the bases of $\mathbb{P}^1_{div}$ and $\mathbb{Q}^1_{div}$ are L^2-orthogonal, the schemes will only require the "inversion" of diagonal local mass matrices. Another advantage is that the orthogonal form of the bases makes the hybridization of schemes very easy to implement. Concerning stability, the numerically observed maximal values of the Courant number $\nu = c\Delta t\sqrt{3}/h$ leading to a stable method on cubes of size h can be compared to the corresponding value for Yee's scheme, for which $\nu = 1$. We have observed numerically that $\nu_{\mathbb{P}^1_{div}} = \nu_{\mathbb{Q}^1_{div}} = 0.65$. An additional **DG**-$\mathbb{P}^2_{div}$ method was considered to get rid of possible numerical reflections at boundaries of a locally refined grid [8].

Divergence preservation. It is clear that Gauss laws are automatically satisfied by transient solutions of Maxwell's equations if they are satisfied at initial time, *i.e.* $\mathrm{div}(\bar{\bar{\varepsilon}}\vec{E}) = \rho$, $\mathrm{div}(\bar{\bar{\mu}}\vec{H}) = 0$, where the density of electric charge ρ verifies $\frac{\partial \rho}{\partial t} = \mathrm{div}(\vec{\mathbf{j}})$. However, since Maxwell equations are only solved in an approximate way, it is very interesting to investigate whether numerical approximations of Gauss laws are verified by the numerical approximate fields. It has been proved that the **DG**-$\mathbb{Q}^1_{div}$ method (2)-(3)-(4) preserves the Gauss divergence laws on a conforming orthogonal hexahedral grid in the following weak sense: the approximate electromagnetic fields $(\vec{\mathbf{E}}_i^n, \vec{\mathbf{H}}_i^{n+1/2})_{i,n}$ verify: $\forall \psi \in \mathbb{Q}^1$ (set of continuous piecewise-affine scalar functions), we have $\vec{\nabla}\psi \in \mathbb{Q}^1_{div}$, $\vec{\mathrm{curl}}\vec{\nabla}\psi \overset{\mathcal{D}'}{=} \vec{0}$, and

$$\int_{\Omega_h} \psi \,\mathrm{div}\, \bar{\bar{\varepsilon}}(\vec{\mathbf{E}}^{n+1} - \vec{\mathbf{E}}^{n}) = \Delta t \int_{\Omega_h} \psi \,\mathrm{div}\, \vec{\mathbf{j}}^{n+1/2}, \quad \int_{\Omega_h} \psi \,\mathrm{div}\, \bar{\bar{\mu}}(\vec{\mathbf{H}}^{n+1/2} - \vec{\mathbf{H}}^{n\text{-}1/2}) = 0.$$

Dispersion analysis. A general dispersion analysis for DGTD methods on Cartesian grids for complete sets of polynomial functional sets has been given by Ainsworth [2]. In the present cases, either with the $\mathbf{DG}-\mathbb{P}^1_{div}$ method or the $\mathbf{DG}-\mathbb{Q}^1_{div}$ method, the polynomial functional sets are not complete and a dispersion analysis can be done by hand in the homogeneous isotropic case on uniform grids. Previous partial results [8] have been completed and the conclusions are quite interesting. For the $\mathbf{DG}-\mathbb{P}^1_{div}$, they can be summed up in the following way [6] in function of the wave vector $\vec{k}=(k_x,k_y,k_z)$ and $h=\max(\Delta x,\Delta y,\Delta z)$ (let us define the constant vector $\vec{s}=(s_x:=\Delta x/h, s_y:=\Delta y/h, s_z:=\Delta z/h)$):

- either $\vec{k}$ is not such that $3k_x=\|\vec{k}\|$ or $3k_y=\|\vec{k}\|$ or $3k_z=\|\vec{k}\|$, and the dispersion relation is of the form $\frac{\omega^2}{|k|^2c^2}=1-2Z(\vec{k},\vec{s})h^2+\frac{k^2c^2\Delta t^2}{12}+o(h^2,\Delta t^2)$, where $Z(\vec{k},\vec{s})$ is bounded when h and Δt go to zero; in that case the relation dispersion shows the plane waves (in the direction $\vec{k}$) are propagated with second-order accuracy; however, the function $Z(\vec{k},\vec{s})$ grows unboundedly when $\vec{k}$ goes near singular directions (see second case);
- or $\vec{k}$ is such that $3k_x=\|\vec{k}\|$ or $3k_y=\|\vec{k}\|$ or $3k_z=\|\vec{k}\|$, and the dispersion relation is of the form $\frac{\omega^2}{|k|^2c^2}=1\pm X(\vec{k},\vec{s})h+\frac{k^2c^2\Delta t^2}{12}+o(h,\Delta t^2)$ which means plane waves in some directions are not propagated with second-order accuracy, and the scheme is first-order accurate.

The form of this result is quite surprising, in particular because the singular directions do not depend on the aspect ratios (*i.e.* $\vec{s}$) of the elements. This should be related in some way to the incompleteness of the DG spaces finite element spaces considered. This is confirmed by the fact that the same dispersion analysis conducted for the $\mathbf{DG}-\mathbb{P}^1$ method (complete set of piecewise affine fields) leads to overall second-order accuracy. Finally, the results are similar for the $\mathbf{DG}-\mathbb{Q}^1_{div}$, which also means that the first-order dispersion in singular directions is not linked to the weak divergence property, only verified by $\mathbf{DG}-\mathbb{Q}^1_{div}$ method.

Anyway, in the computations made with these DG methods, no particular problem was actually encountered with errors in so-called singular directions. The behavior of the methods is similar to comparable DG methods: near the limit of the stability of each scheme, the dispersion errors are really close to each other and comparable to those of the FDTD [36]. Moreover, as the time-step gets smaller, the maximal dispersion does not increase with DG methods (which is not the case of the FDTD).

Non-conforming local refinement. One property of the DG discretization methods is to handle easily non-conforming local refinement of cartesian grids, as well as variations in the local order of accuracy. This allows a dramatic reduction of the number of degrees of freedom required for the treatment of systems with small details. We use here the same approach as in [8]: a coarse grid is used, and locally refined in particular zones of interest. In all elements, the local discretization space used is $\mathbb{Q}^1_{div}$. However, around the selected zones of interest, the order of local approximation can be enhanced to $\mathbb{Q}^2_{div}$ [6] in order to get rid of artificial reflections at the non-conforming interfaces (see Figure 1).

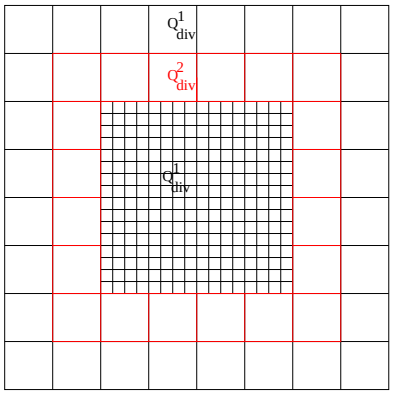

Figure 1: Discretization spaces used in a non-conforming locally refined grid.

3 A Discontinuous Galerkin implementation of UPML

Exterior wave propagation problems have to be set on a bounded domain. The use of an artificial boundary of the domain with an approximately transparent boundary condition can be of dramatic importance for time-domain computations. Absorbing boundary conditions have been constructed since many years for wave propagation problems, with general smooth far-field boundaries [13, 18]. These methods perform very well for plane waves with orthogonal incidence, but more poorly (artificial reflections) as the wave vector gets closer to grazing incidence.

At the same time, the idea to post a material layer around the domain with absorbing properties was also developed. Recently, Bérenger [5] proposed to use layers of a totally artificial, perfectly matched material such that no artificial reflection was present for any plane wave with any incidence at the continuous level. In this method, each component of the perturbed electromagnetic field is split into two artificial subcomponents, making this formulation a split-field formulation, very different from Maxwell equations. The method had a deep impact on the community and was adapted to different engineering problems involving waves [12, 23, 37]. It was also enhanced in many ways, by getting rid of possible unbounded linear growth [1, 4] in particular via so-called unsplit formulations [28, 34, 37], where the equations for perturbed fields can be seen as perturbations of Maxwell equations. This also allows the introduction of metallic conductors through the UPML regions, like an infinite feeding line for instance.

3.1 The UPML continuous formulation

We refer to [34] for the derivation of the UPML method we use in this work. We assume the material is homogeneous and isotropic near the UPML region, *i.e.* $\bar{\bar{\varepsilon}} = \varepsilon\ \mathbb{I}_3$, $\bar{\bar{\mu}} = \mu\ \mathbb{I}_3$. Introducing *a priori* six conductivity parameters defining the artificial material, $(\sigma_s)_{s\in\{x,y,z\}}$ and $(\sigma_s^*)_{s\in\{x,y,z\}}$, the artificial material in the absorbing layer is "perfectly matched" if, for $\forall s \in \{x,y,z\}$, $\sigma_s/\varepsilon = \sigma_s^*/\mu := \bar{\sigma}_s$. Introducing two additional fields $\vec{P}$ and $\vec{Q}$, and two perturbed electromagnetic fields $(\vec{\tilde{E}}, \vec{\tilde{H}})$, defined by

$$\forall s \in \{x,y,z\},\ \tilde{E}_s = E_s + \bar{\sigma_s} P_s,\ \tilde{H}_s = H_s + \bar{\sigma_s} Q_s, \tag{5}$$

the UPML equations read

$$\left\{ \begin{array}{l} \partial_t \vec{\tilde{E}} + R\vec{\tilde{E}} + S\vec{P} = \frac{1}{\varepsilon}\ \vec{\text{curl}}\ \vec{\tilde{H}}, \\ \partial_t \vec{P} + N\vec{P} - \vec{\tilde{E}} = 0, \end{array} \right. \quad \left\{ \begin{array}{l} \partial_t \vec{\tilde{H}} + R\vec{\tilde{H}} + S\vec{Q} = -\frac{1}{\mu}\ \vec{\text{curl}}\ \vec{\tilde{E}}, \\ \partial_t \vec{Q} + N\vec{Q} - \vec{\tilde{H}} = 0, \end{array} \right. \tag{6}$$

where the matrices R, S, and N are three 3×3 diagonal matrices, given by

$$\left\{ \begin{array}{rcl} R & = & \text{diag}\left[\ \bar{\sigma}_y + \bar{\sigma}_z - \bar{\sigma}_x,\ \bar{\sigma}_x + \bar{\sigma}_z - \bar{\sigma}_y,\ \bar{\sigma}_x + \bar{\sigma}_y - \bar{\sigma}_z\right], \\ S & = & \text{diag}\left[\ (\bar{\sigma}_x - \bar{\sigma}_y)(\bar{\sigma}_x - \bar{\sigma}_z),\ (\bar{\sigma}_y - \bar{\sigma}_x)(\bar{\sigma}_y - \bar{\sigma}_z),\ (\bar{\sigma}_z - \bar{\sigma}_x)(\bar{\sigma}_z - \bar{\sigma}_y)\right], \\ N & = & \text{diag}\left[\ \bar{\sigma}_x,\ \bar{\sigma}_y,\ \bar{\sigma}_z\right]. \end{array} \right. \tag{7}$$

One can easily notice that, away from the UPML regions, where all artificial conductivities $\bar{\sigma}_s$ are zero, the perturbed fields are equal to the physical electromagnetic fields (*i.e.* $\vec{\tilde{E}} = \vec{E}$ and $\vec{\tilde{H}} = \vec{H}$), and they are solutions of the original Maxwell equations.

3.2 DG space discretization of the UPML formulation

In each finite element $\mathcal{T}_i$, the numerical unknowns are doubled (actually, only in UPML regions). They correspond to components of the fields $(\vec{\tilde{E}},\ \vec{\tilde{H}},\ \vec{P},\ \vec{Q})$ on the local bases of fields $\vec{\varphi}_{ij}$, $1 \le j \le d_i$ (in the sequel, the $\tilde{}$ symbols will be omitted). For clarity, we recall that:

$$\forall \vec{x} \in \mathcal{T}_i, \left\{ \begin{array}{rcl} \vec{E}_i(\vec{x}) & = & \sum_{j=1}^{d_i} E_{ij} \vec{\varphi}_{ij}(\vec{x}), \\ \vec{H}_i(\vec{x}) & = & \sum_{j=1}^{d_i} H_{ij} \vec{\varphi}_{ij}(\vec{x}), \\ \vec{Q}_i(\vec{x}) & = & \sum_{j=1}^{d_i} Q_{ij} \vec{\varphi}_{ij}(\vec{x}), \\ \vec{P}_i(\vec{x}) & = & \sum_{j=1}^{d_i} P_{ij} \vec{\varphi}_{ij}(\vec{x}). \end{array} \right.$$

Then, using these approximations, multiplying (6) by any basis function $\vec{\varphi}_{ij}$, integrating over the element $\mathcal{T}_i$, integrating by parts, and using the centered flux approximation for surface integrals, we get [6] in matricial form:

$$\left\{\begin{array}{rcl} \mathbb{M}_i\dfrac{\partial \mathbf{E}_i}{\partial t}+\mathbb{R}_i\mathbf{E}_i+\mathbb{S}_i\mathbf{P}_i & = & \dfrac{1}{\varepsilon}(\mathbb{A}_i\mathbf{H}_i-\displaystyle\sum_{k\in\mathcal{V}_i}\mathbb{F}_{ik}\mathbf{H}_k) \\ \mathbb{M}_i\dfrac{\partial \mathbf{P}_i}{\partial t}+\mathbb{N}_i\mathbf{P}_i-\mathbb{M}_i\mathbf{E}_i & = & 0 \\ \mathbb{M}_i\dfrac{\partial \mathbf{H}_i}{\partial t}+\mathbb{R}_i\mathbf{H}_i+\mathbb{S}_i\mathbf{Q}_i & = & \dfrac{1}{\mu}(-\mathbb{A}_i\mathbf{E}_i+\displaystyle\sum_{k\in\mathcal{V}_i}\mathbb{F}_{ik}\mathbf{E}_k) \\ \mathbb{M}_i\dfrac{\partial \mathbf{Q}_i}{\partial t}+\mathbb{N}^i\mathbf{Q}_i-\mathbb{M}_i\mathbf{H}_i & = & 0 \end{array}\right. \tag{8}$$

where we have used the following notations:

- $\mathbf{X}_i$ is the column-vector $(X_{il})_{l=1,d_i}$, for $X\in\{H,E,Q,P\}$;
- $\mathbb{M}_i$ is the local s.p.d. $d_i\times d_i$ mass matrix, with $\mathbb{M}^i[j,l]=\int_{\mathcal{T}_i}\vec{\varphi}_{ij}\cdot\vec{\varphi}_{il}$
- $\mathbb{A}_i$ is a square $(d_i\times d_i)$ matrix, with $\mathbb{A}^i[j,l]=\frac{1}{2}\int_{\mathcal{T}_i}[\vec{rot}\vec{\varphi}_{il}\cdot\vec{\varphi}_{ij}+\vec{rot}\vec{\varphi}_{ij}\cdot\vec{\varphi}_{il}]$
- for $\mathcal{T}_k$ neighboring $\mathcal{T}_i$, $\mathbb{F}_{ik}$ is a rectangular $(d_i\times d_k)$ flux matrix, with $\mathbb{F}_{ik}[j,l]=\frac{1}{2}\int_{a_{ik}}(\vec{\varphi}_{ij}\times\vec{\varphi}_{kl})\cdot\vec{n_{ik}}$
- $\mathbb{R}_i$, $\mathbb{S}_i$, $\mathbb{N}_i$ are three square $(d_i\times d_i)$ matrices, with $\mathbb{Z}^i[j,l]=\int_{\mathcal{T}_i}Z\vec{\varphi}_{ij}\cdot\vec{\varphi}_{il}$, for $Z\in\{R,S,N\}$;

3.3 Time-discretization of the discrete UPML formulation

Introducing the variables $\mathbf{X}_i$ and $\mathbf{Y}_i$ in $\mathbb{R}^{2d_i}$ and the square $(2d_i)\times(2d_i)$ matrix $\mathbb{U}_i$ defined by:

$$\mathbf{X}_i=\left(\begin{array}{c}\mathbf{E}_i\\ \mathbf{P}_i\end{array}\right),\ \mathbf{Y}_i=\left(\begin{array}{c}\mathbf{H}_i\\ \mathbf{Q}_i\end{array}\right),\ \mathbb{U}_i=\left(\begin{array}{cc}\mathbb{M}_i^{-1}\mathbb{R}_i & \mathbb{M}_i^{-1}\mathbb{S}_i\\ -\mathbb{I}d & \mathbb{M}_i^{-1}\mathbb{N}_i\end{array}\right), \tag{9}$$

equations (8) take the form

$$\left\{\begin{array}{rcl} \dfrac{\partial \mathbf{X}_i}{\partial t}+\mathbb{U}_i\mathbf{X}_i & = & \dfrac{1}{\varepsilon}\mathbb{M}_i^{-1}\left(\begin{array}{c}\mathbb{A}_i\mathbf{H}_i-\sum_{k\in\mathcal{V}_i}\mathbb{F}_{ik}\mathbf{H}_k\\ 0\end{array}\right) \\ \dfrac{\partial \mathbf{Y}_i}{\partial t}+\mathbb{U}_i\mathbf{Y}_i & = & \dfrac{1}{\mu}\mathbb{M}_i^{-1}\left(\begin{array}{c}-\mathbb{A}_i\mathbf{E}_i+\sum_{k\in\mathcal{V}_i}\mathbb{F}_{ik}\mathbf{E}_k\\ 0\end{array}\right) \end{array}\right. \tag{10}$$

We chose to use a leap-frog type time-integration scheme for the terms in the right-hand side of the equations, with an exponential time-scheme for the loss-type terms in the left-hand side. Electric fields $\mathbf{X}_i$ (thus $\mathbf{E}_i$ and $\mathbf{P}_i$) are computed at integer time-stations, while magnetic fields $\mathbf{Y}_i$ (thus $\mathbf{H}_i$ and $\mathbf{Q}_i$) are computed at half-integer time-stations. The time-scheme reads:

$$\left\{\begin{array}{rcl} \mathbf{X}_i^{n+1} & = & e^{-\mathbb{U}_i\Delta t}\mathbf{X}_i^n+\dfrac{1}{\varepsilon}\left(\displaystyle\int_0^{\Delta t}e^{-\mathbb{U}_i s}\,ds\right)\ \mathbb{M}_i^{-1}\ \left(\begin{array}{c}\mathbb{A}_i\mathbf{H}_i^{n+1/2}-\sum_{k\in\mathcal{V}_i}\mathbb{F}_{ik}\mathbf{H}_k^{n+1/2}\\ 0\end{array}\right) \\ \mathbf{Y}^{n+3/2} & = & e^{-\mathbb{U}_i\Delta t}\mathbf{Y}_i^{n+1/2}-\dfrac{1}{\mu}\left(\displaystyle\int_0^{\Delta t}e^{-\mathbb{U}_i s}\,ds\right)\ \mathbb{M}_i^{-1}\ \left(\begin{array}{c}\mathbb{A}_i\mathbf{E}_i^{n+1}-\sum_{k\in\mathcal{V}_i}\mathbb{F}_{ik}\mathbf{E}_k^{n+1}\\ 0\end{array}\right). \end{array}\right. \tag{11}$$

The stability and the applicability of the scheme proposed depends on the properties of the matrices $\mathbb{U}_i$ (it is clear that, away from PML regions, we recover the leap-frog time-scheme, which is stable under a CFL-like stability condition). The computation of the exponentials of matrices used in the scheme above are easy as long as the matrices $\mathbb{U}_i$ are diagonalizable, which is the case if $\bar{\sigma}_x\neq\bar{\sigma}_y\neq\bar{\sigma}_z\neq\bar{\sigma}_x$. We have used classical profiles for the artificial conductivities, *i.e.* $\sigma_s(x,y,z)=(1+\alpha_s)\sigma_m[s/\xi]^n$, where s denotes the space coordinate along the s-axis starting at the inside boundary of the UPML region,

ξ is the thickness of the UPML region, $n = 2$ yields a parabolic profile for the conductivity, and σ_m represents the maximal conductivity at the exterior boundary. The global reflection coefficient of the UPML region is related to this parameter σ_m [6]. In UPML "corner" and "edge" regions (*i.e.* where two or three conductivity coefficients are non-zero), α_x, α_y and α_z are chosen small if necessary and such that $\bar{\sigma}_x \neq \bar{\sigma}_y \neq \bar{\sigma}_z \neq \bar{\sigma}_x$ in all UPML elements. If one or less conductivity $\bar{\sigma}_s$ is non zero (*i.e.* in the central domain and in UPML "face" regions), it is preferred not to use the corresponding components of the additional fields $\vec{P}$ and $\vec{Q}$, since it can be shown their contributions vanish in (6) for what concerns the time evolution of electromagnetic fields $\vec{E} \equiv \vec{\tilde{E}}$ and $\vec{H} \equiv \vec{\tilde{H}}$.

Finally, on the exterior boundary of the UPML region, a simple reflecting metallic boundary condition is used (letting reflected waves being absorbed another time in their way back through the UPML regions).

3.4 Numerical assessment on planar structures

In this section, we assess the time and space discretizations schemes on simple numerical test-cases involving planar structures. First, an infinite transmission line is simulated and its radiation pattern and impedance bandwidth are evaluated; then a patch antenna (with air or dielectric substrates) is connected to the transmission line and numerically characterized.

Numerical analysis of an infinite transmission line. The micro-strip transmission line considered is set over a dielectric substrate ($\varepsilon_r = 1$, thickness $h = 0.794\ mm$, width $W = 2.46\ mm$) with a metallic ground plane. Instead of exciting the micro-strip line in a transverse plane [19, 33] via the vertical (normal to the strip plane) component E_z of the electric field, a vertical source current $\vec{J} = J_z \vec{e}_z$ in the frequency band 10-20 GHz is used, J_z being a sine-modulated Gaussian of the form: $J_z = J_0\, e^{(t-t_0)^2/T^2} \sin(2\pi f_0(t-t_0))$ with $J_0 = 1\ A/m^2$, $t_0 = 2.14\ T$, and $T = 0.483/f_{max}$ with f_{max} =22 GHz. In the DG-$\mathbb{Q}^1_{div}$ framework, the excitation is taken into account for the degrees of freedom corresponding to vertical edges in the excitation plane. The infinite micro-strip line is simulated by surrounding it in UPML regions, with both ends embedded in UPML regions (see Figure 2). The brick elements are in this case cubes with

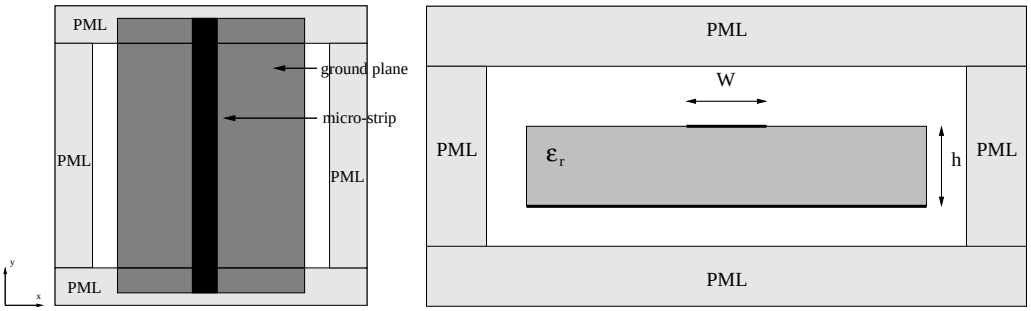

Figure 2: Infinite micro-strip line from above (left) and in the excitation plane (right).

edge $\Delta x = \Delta y = \Delta z = 0.265\ mm$, corresponding to nine elements in the line width W and three in the substrate thickness h. The 6-cell thick UPML regions are set at two cells away from the line in the $0x$ and $0z$, direction, with parabolic profile for the artificial conductivities.

The calculation of the characteristic impedance $Z_c(f) = V(f)/I(f)$ and the propagation constant $\beta(f)$ in function of the frequency requires the computation of Fourier transforms of the potential difference $V(f)$ under the line (below the center) and the electric current $I(f)$ inside the line, obtained via contour integration of the magnetic field around the line (on a plane parallel to the excitation plane, sufficiently far away from the excitation plane). This can be done by choosing the correct degrees of freedom in the DG-$\mathbb{Q}^1_{div}$ formulation (see Figure 3). The computation of $Z_c(f)$ requires particular numerical treatment in the context of numerical simulations with the FDTD [19, 33], because degrees of freedom related to the electric and magnetic fields cannot be located in the same vertical plane. On the contrary, this is the case in the DG-$\mathbb{Q}^1_{div}$ context. However, since both fields are not evaluated at

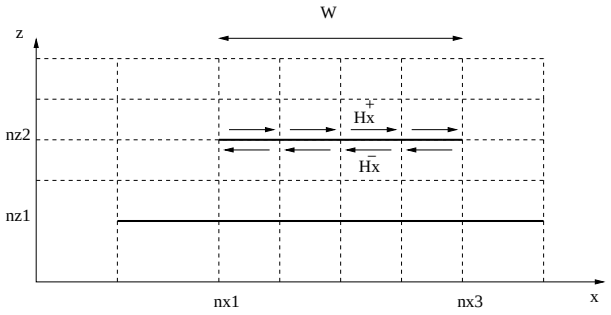

Figure 3: Transverse section of the feeding line and integration contour of the magnetic field.

the same times (leap-frog time-scheme), a time correction is also considered here, for example by using $I^{cor}(f) = I(f)e^{i\omega\frac{\Delta t}{2}}$ instead of $I(f)$. Empirical formulas for $Z_c(f)$ [32] yield $\Re(Z_0^{ref}) = 68.9\ \Omega$ and $\Im(Z_0^{ref}) = 0\ \Omega$. The computed values drawn on Figure 4 show a very good agreement with the expected values (in particular, $|Z_0 - Z_0^{ref}| \leq 1.4\ \Omega$ and $|Z_0 - Z_0^{ref}| \leq 0.5\ \Omega$ in the range 15-20 GHz).

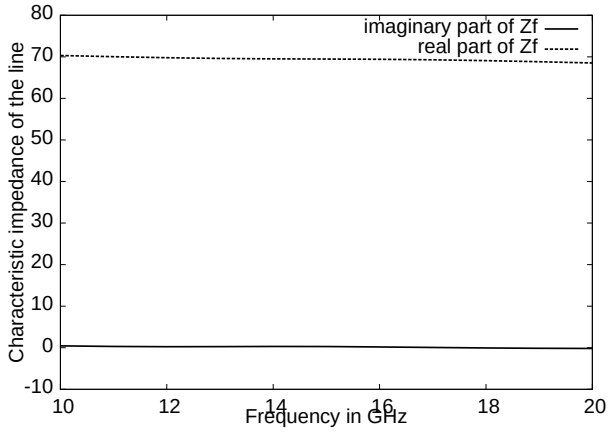

Figure 4: $Z_0(f)$ after time correction (real part in continuous line, imaginary part in dashed line).

Numerical analysis of an infinite transmission line with local refinement. We consider now the same test case with a locally-refined grid and aim at evaluating the possible reflection inside the micro-strip transmission line due to the local non-conforming refinement. Therefore, we compute the reflection coefficient (S_{11}) and the standing wave ratio (SWR) for a transmission line going through a refined zone $[0; 13.25] \times [10.6; 13.25] \times [0; 13.25]$ (in mm, the whole domain being $[0; 13.25] \times [0; 26.5] \times [0; 13.25]$). The refinement ratios considered are 1 (*i.e.* no refinement), 2, 4, and 8. Views of the corresponding grids are shown on Figure 5. The computed values for the S_{11} (in dB) and SWR coefficients are shown on Figure 6. They compare very well with the expected values (0 and 1 respectively).

Numerical analysis of a patch antenna. We compute numerically the coefficients S_{11} and SWR for a rectangular patch antenna with a substrate equivalent to air ($\varepsilon_r = 1$). The patch is directly fed by an asymmetric feeding line (see Figure 7). The computational domain $23,820\ mm \times 33,348\ mm \times 7,94\ mm$ is first uniformly meshed with $\Delta x = \Delta y = \Delta z = 0,265\ mm$. The patch is excited via a dipole (with the same characteristics as previously). The reflection coefficient S_{11} is directly accessible since the incident tension has been computed for the transmission line only (*i.e.* $S_{11}(f) = (\hat{V}_{tot}(t) - \hat{V}_i(t))/\hat{V}_i(t)$). The values of S_{11} and the standing wave ratio SRW (given by SWR $= (1 + |S_{11}|)/(1 - |S_{11}|)$) are compared on Figure 8 with results obtained by a standard FDTD and by the software HFSS [21] (considered as reference). The numerical results of the DGTD-$\mathbb{Q}^1_{div}$ method are in good agreement with those of HFSS.

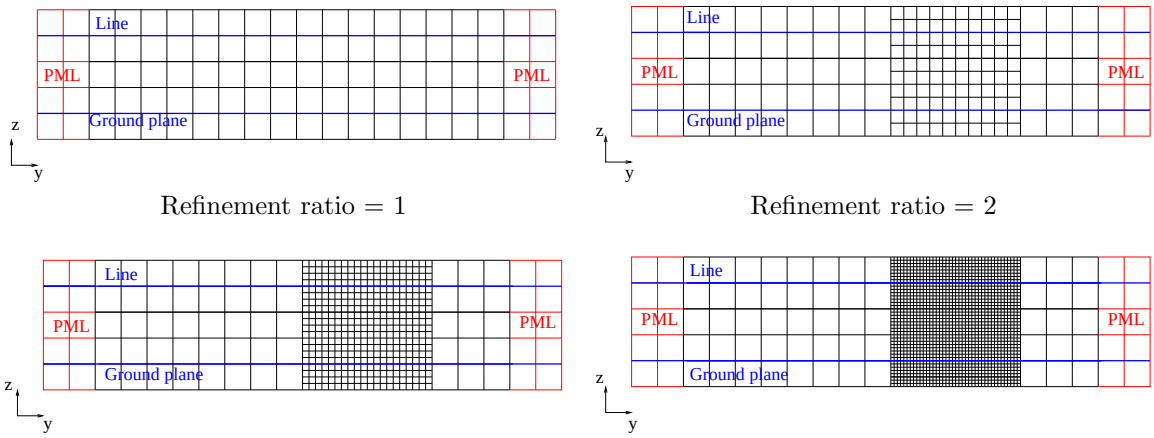

Figure 5: The transmission line and the locally-refined grids

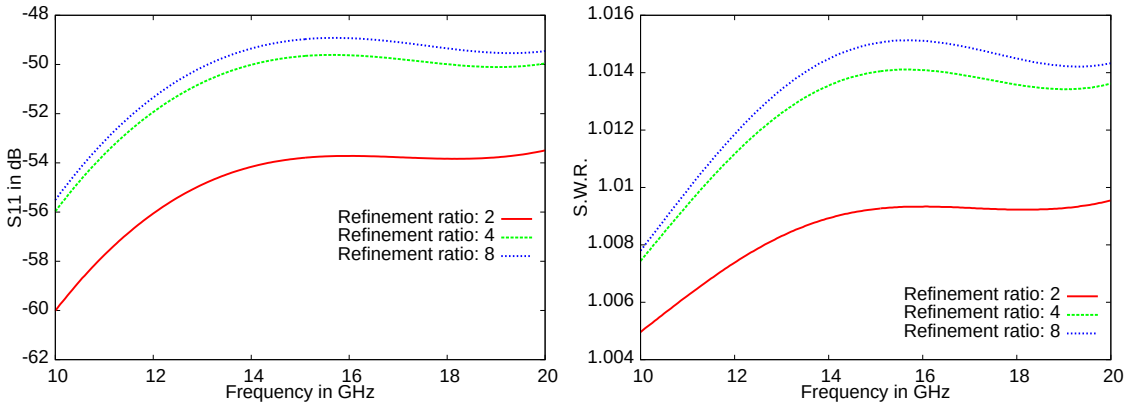

Figure 6: S_{11} and SWR coefficients for different refinement ratios $k_x = k_y = k_z = 2, 4, 8$

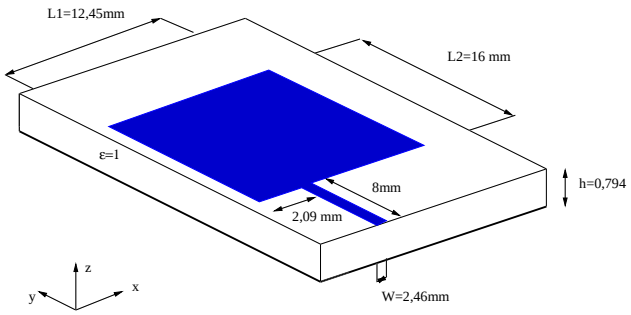

Figure 7: Patch antenna fed by a micro-strip line.

Numerical analysis of a patch antenna with local refinement. In order to obtain a better accuracy in a region close to the patch and the line, we consider now the same configuration with a locally refined cartesian grid. The patch and the line are completely included in the refined zone, as described in Figure 9. The computational domain $23,820\ mm \times 33,348\ mm \times 7,94\ mm$ is uniformly meshed with $\Delta x = \Delta y = \Delta z = 0,794\ mm$ and refined (cell dimensions are divided by 4 in all three directions, thus $\Delta x_r = \Delta y_r = \Delta z_r = 0,1985\ mm$) in a $12,704\ mm \times 23,82\ mm \times 1,588\ mm$ zone around the antenna and the line. Therefore, the mesh is finer than the reference uniform grid near the patch antenna, and coarser outside the refined box. The total number of elements in the locally refined mesh,

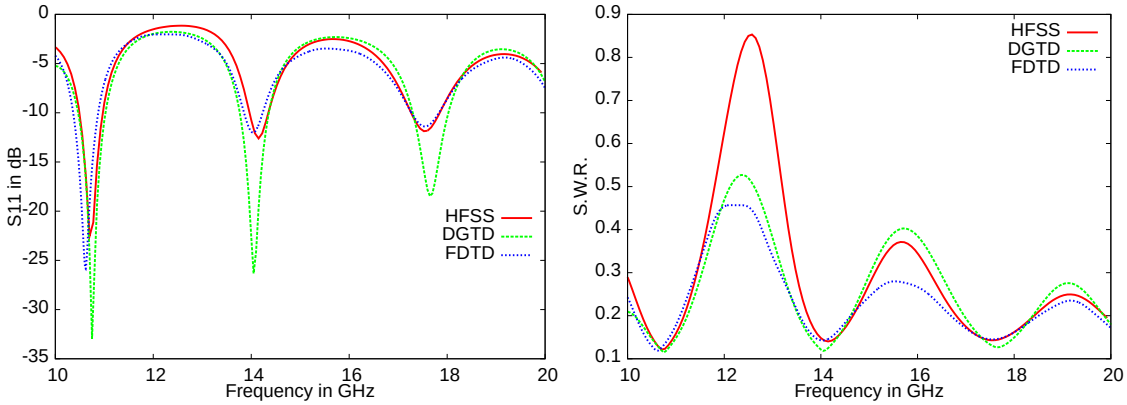

Figure 8: Values of $|S_{11}(f)|$ (left) and SWR(f) (right) computed using: (green) DGTD-$\mathbb{Q}^1_{div}$; (blue) FDTD; (red) HFSS.

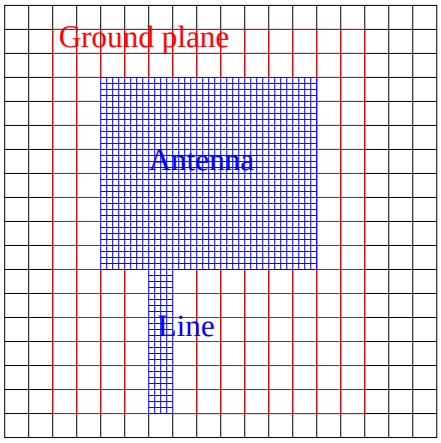

Figure 9: Locally refined non conforming mesh for the patch antenna.

here approximately 73k, is to be compared with the number of elements of the uniform mesh with $\Delta x = \Delta y = \Delta z = 0,1985\ mm$, approximately 806k elements, and with the reference uniform mesh with $\Delta x = \Delta y = \Delta z = 0,265\ mm$, approximately 340k elements. The values of S_{11} are compared on Figure 10 with results obtained by a standard FDTD on the fine reference uniform mesh (with $\Delta x = \Delta y = \Delta z = 0,265\ mm$) and by the software HFSS (considered as reference). The numerical results computed on the locally refined mesh with the DGTD-$\mathbb{Q}^1_{div}$ method compare very well at least, indeed get closer than those obtained with the FDTD to those obtained by HFSS.

4 A fictitious domain approach based on a DG method

The fictitious domain approaches have been introduced in order to replace the solution of a system of PDEs outside geometrically complex domain with physical boundary conditions on its boundaries, by a locally modified (in general by a local source term) system of PDEs in a geometrically simple domain, for example a parallelepipedic part of $\mathbb{R}^d$. Amongst many approaches (see for other types of approaches), the most popular point of view in the domain of wave propagation problems is based on Lagrange multipliers [3] and the solution of a saddle-point problem [16, 17, 35]. Boundary conditions are set in a weak way, which allows the joint use of a cartesian volumic grid and a surfacic (possibly triangular) mesh for the physical boundary.

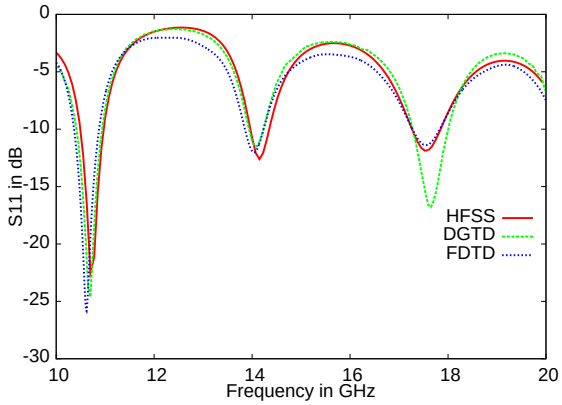

Figure 10: Values of $|S_{11}(f)|$ computed using: (green) DGTD-$\mathbb{Q}^1_{div}$; (blue) FDTD; (red) HFSS.

4.1 A standard fictitious domain method for the Maxwell equations

Let us denote by Ω_i the volumic domain occupied by a metallic perfect conductor, with Γ its regular boundary, and $\Omega_{ex} = \Omega/\bar{\Omega}_i$ the exterior domain. In the fictitious domain approach [15], the time-domain Maxwell equations on $\Omega \times \mathbb{R}^+$ are replaced by the new set of equations, according to:

$$\left| \begin{array}{l} \text{Find } (\vec{E},\vec{H}) \text{ in } H(\vec{\text{curl}},\Omega_{ex}) \text{ such that} \\ \left\{ \begin{array}{ll} \varepsilon_0 \partial_t \vec{E} - \vec{\text{curl}}\vec{H} = 0 & \text{on } \Omega_{ex}, \\ \mu_0 \partial_t \vec{H} + \vec{\text{curl}}\vec{E} = 0 & \text{on } \Omega_{ex}, \\ \vec{E} \times \vec{n} = 0 & \text{on } \Gamma, \end{array} \right. \end{array} \right. \longrightarrow \left| \begin{array}{l} \text{Find } (\vec{E},\vec{H}) \text{ in } H(\vec{\text{curl}},\Omega) \text{ and} \\ \vec{j} \text{ in } H^{-1/2}(\text{div}_\Gamma,\Gamma) \text{ such that} \\ \left\{ \begin{array}{l} \varepsilon_0 \partial_t \vec{E} - \vec{\text{curl}}\vec{H} + B^*\vec{j} = 0 \\ \mu_0 \partial_t \vec{H} + \vec{\text{curl}}\vec{E} = 0 \\ B\vec{E} = 0 \end{array} \right. \end{array} \right. \tag{12}$$

where $H(\vec{\text{curl}},\Omega) := \{\vec{v} \in L^2(\Omega)^3,\ \vec{\text{curl}}\ \vec{v} \in L^2(\Omega)^3\}$, $H^{-1/2}(\Gamma)$ is a trace space containing the tangential components of $H(\vec{\text{curl}},\Omega)$ fields, $H^{-1/2}(\text{div}_\Gamma,\Gamma) = \{\vec{\mu} \in H^{-1/2}(\Gamma)^2, \text{div}_\Gamma\, \vec{\mu} \in H^{-1/2}(\Gamma)^2\}$ is a subspace of $H^{-1/2}(\Gamma)$, on which one can define the bilinear form $b\ :\ H(\vec{\text{curl}},\Omega) \times H^{-1/2}(\text{div}_\Gamma,\Gamma) \longrightarrow \mathbb{R}$ by

$$b(\vec{E},\vec{j}) := \int_\Gamma \Big((\vec{E}_h \times \vec{n}) \times \vec{n} \Big) \cdot \vec{j}.$$

Finally, using the duality between $H^{-1/2}(\vec{\text{curl}}_\Gamma,\Gamma)$ and $H^{-1/2}(\text{div}_\Gamma,\Gamma)$, the linear operator B from $H(\vec{\text{curl}},\mathbb{R}^3)$ into $H^{-1/2}(\vec{\text{curl}}_\Gamma,\Gamma)$ (and its adjoint B^*) are defined by duality by: $\forall \vec{E} \in H(\vec{\text{curl}},\mathbb{R}^3), \forall \vec{j} \in H^{-1/2}(\text{div}_\Gamma,\Gamma)$, $< B\vec{E},\vec{j} >=< \vec{E},B^*\vec{j} >:= b(\vec{E},\vec{j})$.

Properties of the formulation. The well-posedness of the new formulation in (12) has been established in [15] (assuming compatibility relations on the initial conditions). It uses an "inf-sup" condition on the continuous spaces, *i.e.* there exists $k > 0$ such that

$$\inf_{\vec{j} \in H^{-1/2}(\text{div}_\Gamma,\Gamma)} \left[\sup_{\vec{E} \in H(\text{curl},\Omega)} \left(\frac{b(\vec{E},\vec{j})}{||\vec{E}||_{H(\vec{\text{curl}},\Omega)} ||\vec{j}||_{H^{-1/2}(\text{div}_\Gamma,\Gamma)}} \right) \right] \geq k \tag{13}$$

It is also proved that the energy of the solution is constant in time (provided the initial compatibility relations are verified).

Convergence of the semi-discretization in space. The semi-discretization in space, in a finite element analysis sense, starts with the choices of subspaces of $H(\vec{\text{curl}},\Omega)$ and $H^{-1/2}(\text{div}_\Gamma,\Gamma)$ of finite dimensions (assuming a volumic grid and a surfacic triangular mesh are given). In the case where the "inf-sup" condition (13) holds on the subspaces with a bound on the constant k independent of the size of the

meshes, the convergence of the formulation (12) is proved (see [3] for the wave equations and [15] for Maxwell equations). However, there seem to remain a *mesh compatibility condition* between the size of the cartesian grid elements and the size of the triangles in the metallic surfacic mesh. A theoretical result was given by Girault and Glowinski in [35] for the waves equations, which was qualitatively confirmed for Maxwell equations [15]: if h denotes the grid size for the volumic cartesian grid, and h' denotes the size of the smallest triangular element in the surfacic triangulation, then the condition $h \leq h'$ should be verified. This condition implies that a small detail in the surfacic mesh will make mandatory the use of a very fine volumic grid, leading to prohibitive computational requirements. We aim now at mixing a fictitious domain approach with locally-refined DGTD methods.

4.2 A DGTD fictitious domain method for the Maxwell equations

Space discretization. We intend to use the DGTD method presented in Section 2.2. The electric and magnetic fields are seeked for in the finite dimensional space $\mathbb{Q}^1_{div}$, which makes the approximation non-conformal in the finite element sense (*i.e.* $\mathbb{Q}^1_{div} \not\subset H(\vec{\text{curl}}, \Omega)$). Thus, the bilinear form $b(\vec{E}, \vec{j})$ is not well-defined for $\vec{E} \in H(\vec{\text{curl}}, \Omega)$. The idea is then to use some projection operator A from $\mathbb{Q}^1_{div}$ onto $H(\vec{\text{curl}}, \Omega)$ and to consider the following DGTD fictitious domain formulation: find $(\vec{E_h}, \vec{H_h}) \in \mathbb{V}_h \times \mathbb{V}_h$ with $\mathbb{V}_h = \{\vec{\mathbf{V}}_h \in L^2(\Omega)^3 | \forall i,\ \vec{\mathbf{V}}_{h|\mathcal{T}_i} \in \mathbb{Q}^1_{div}(\mathcal{T}_i)\}$, and $\vec{j_{h'}} \in \mathbb{J}_{h'}$ ($\mathbb{J}_{h'}$ being a subspace of $H^{-1/2}(\text{div}_\Gamma, \Gamma)$) such that, $\forall E^* \in \mathbb{V}_h$, $\forall H^* \in \mathbb{V}_h$, $\forall j^* \in \mathbb{J}_{h'}$,

$$\left\{ \begin{array}{l} \varepsilon_0(\partial_t \vec{E}_h, \vec{E}^*_h) - (\vec{\text{curl}}_{DG} \vec{E}^*_h, \vec{H}_h) + b\Big(A(\vec{E}^*_h), \vec{j}_{h'}\Big) = 0, \\ \mu_0(\partial_t \vec{H}_h, \vec{H}^*_h) + (\vec{\text{curl}}_{DG} \vec{E}_h, \vec{H}^*_h) = 0, \\ b\Big(A(\vec{E}_h), \vec{j}^*_{h'}\Big) = 0, \end{array} \right. \tag{14}$$

where initial conditions have been omitted. The $\vec{\text{curl}}_{DG}$ operators denotes the DG space discretization of the $\vec{\text{curl}}$ operator introduced in equations 2 (totally centered fluxes). In a compact form, the DG-fictitious domain method above can be rewritten [6] in the compact form:

$$\left\{ \begin{array}{lcl} \varepsilon \mathbb{M}\mathbb{E}_t + \mathbb{L}\mathbb{H} & = & -\mathbb{B}\mathbb{J} \\ \mu \mathbb{M}\mathbb{H}_t - {}^t\mathbb{L}\mathbb{E} & = & 0 \\ {}^t\mathbb{B}\mathbb{E} & = & 0 \end{array} \right. \tag{15}$$

where all unknowns related to the electric (resp. magnetic) field are regrouped in a column vector $\mathbb{E}$ (resp. $\mathbb{H}$), the matrix $\mathbb{M}$ is the block-diagonal mass matrix induced by the Discontinuous Finite element basis $((\vec{\varphi_{ij}})_{1 \leq j \leq d_i})_{\mathcal{T}_i \in \Omega_h}$, $\mathbb{J} = (j_1, \ldots, j_{n_s})^t$ denotes the column vector of degrees of freedom for the surfacic current, *i.e.* $\vec{j}_{h'} = \sum_{s=1}^{n_s} j_s \vec{S}_s$, where $(\vec{S}_s)_{1 \leq s \leq n_s}$ is a basis for the subspace $\mathbb{J}_{h'}$ of $H^{-1/2}(\text{div}_\Gamma, \Gamma)$, and finally $\mathbb{B}$ is a $d \times n_s$ (with $d = \sum_i d_i$) matrix with general term $\mathbb{B}_{(ij,s)} = \int_\Gamma \big(\big(A(\vec{\varphi}_{ij}) \times \vec{n}_\Gamma\big) \times \vec{n}_\Gamma\big) \cdot \vec{S}_s$. Here, we have chosen for the surfacic current the Raviart-Thomas two-dimensional edge elements of lowest degree. n_s is the number of edges in the triangulation and degrees of freedom for $\vec{j}_{h'}$ are fluxes through each edge. In the case where there is no metallic fictitious boundary, the matrix $\mathbb{B}$ vanishes and we recover the standard compact Hamiltonian form for a DG discretization.

Time-discretization and algorithm. It is easy to show that the solutions of the space semi-discretized equations (15) have a constant electromagnetic energy $\mathcal{E} = (\varepsilon {}^t\mathbb{H}\mathbb{M}\mathbb{H} + \mu {}^t\mathbb{E}\mathbb{M}\mathbb{E})/2$. This property can be conserved with the following leap-frog time-integration algorithm:

$$\left\{ \begin{array}{ll} 1. & \text{Find } \mathbb{J}^{n+1/2} \text{ such that } {}^t\mathbb{B}\mathbb{E}^{n+1} = 0, \text{ where} \\ & \mathbb{E}^{n+1} = \mathbb{E}^n - \frac{\Delta t}{\varepsilon}\mathbb{M}^{-1}(\mathbb{L}\mathbb{H}^{n+1/2} + \mathbb{B}\mathbb{J}^{n+1/2}), \\ 2. & \mathbb{H}^{n+3/2} = \mathbb{H}^{n+1/2} + \frac{\Delta t}{\mu}\mathbb{M}^{-1}\mathbb{L}\mathbb{E}^{n+1}. \end{array} \right. \Leftrightarrow \left\{ \begin{array}{ll} 1. & \tilde{\mathbb{E}}^{n+1} = \mathbb{E}^n - \frac{\Delta t}{\varepsilon}\mathbb{M}^{-1}\mathbb{L}\mathbb{H}^{n+1/2}, \\ 2. & \text{Find } \mathbb{K} \mid ({}^t\mathbb{B}\mathbb{M}^{-1}\mathbb{B})\mathbb{K} = -{}^t\mathbb{B}\tilde{\mathbb{E}}^{n+1} \\ 3. & \mathbb{E}^{n+1} = \tilde{\mathbb{E}}^{n+1} + \mathbb{M}^{-1}\mathbb{B}\mathbb{K} \\ 4. & \mathbb{H}^{n+3/2} = \mathbb{H}^{n+1/2} + \frac{\Delta t}{\mu}\mathbb{M}^{-1}\mathbb{L}\mathbb{E}^{n+1}. \end{array} \right. \tag{16}$$

The matrix ${}^t\mathbb{B}\mathbb{M}^{-1}\mathbb{B}$ involved in the linear system of step 2 should be regular. It is clearly symmetric and positive. The choice of the projection operator A must be done such that the matrix is definite. We

choose for the operator A an orthogonal projection onto the finite-dimensional subspace $\mathbb{A}_h$ of $H(\vec{\text{curl}}, \Omega)$ obtained by using the Nédélec lowest-order edge elements [27]. $\mathbb{A}_h = \{\vec{v} = (v_x, v_y, v_z),\ v_x \in Q_{0,1,1},\ v_y \in Q_{1,0,1},\ v_z \in Q_{1,1,0}\}$ and we have indeed $\mathbb{A}_h \subset \mathbb{V}_h$. It is well known that the standard FDTD method can be interpreted as a finite-element formulation with mass condensation, itself being equivalent to the use of a different scalar product on $\mathbb{A}_h$. In order to keep some compatibility with the more standard FDTD-based fictitious domain approach, we define A as the orthogonal projection onto $\mathbb{A}_h$ for the scalar product $< .,. >_\alpha$ ($\alpha > 0$) on $\mathbb{V}_h$ defined by

$$< \vec{U}, \vec{V} >_\alpha = < \vec{U}, \vec{V} >_{\mathbb{A}_h} + \sum_{\substack{Faces \\ \mathcal{T}_i \bigcap \mathcal{T}_j}} \int_{\mathcal{T}_i \bigcap \mathcal{T}_j} [\![\vec{U}]\!][\![\vec{V}]\!] \tag{17}$$

where $[\![\vec{U}]\!]$ denotes the jump of the tangential component of the vector field $\vec{U}$ and $< \vec{U}, \vec{V} >_{\mathbb{A}_h}$ is the standard mass condensation for the FDTD, *i.e.*

$$< \vec{U}, \vec{V} >_{\mathbb{A}_h} = \frac{\Delta x \Delta y \Delta z}{4} \sum_{(i,j,k)} \left[U^x_{i,j-\frac{1}{2},k-\frac{1}{2}} V^x_{i,j-\frac{1}{2},k-\frac{1}{2}} + U^y_{i-\frac{1}{2},j,k-\frac{1}{2}} V^y_{i-\frac{1}{2},j,k-\frac{1}{2}} + U^z_{i-\frac{1}{2},j-\frac{1}{2},k} V^z_{i-\frac{1}{2},j-\frac{1}{2},k} \right].$$

The reader can check [6] that $< .,. >_\alpha$ is actually a scalar product, which extends the FDTD mass condensation over $\mathbb{V}_h$. One can also check that, for a given field $\vec{E}_h$ in $\mathbb{V}_h$, then $A(\vec{E}_h) \in \mathbb{A}_h$ does not depend on α and its degree of freedom attached to a given edge in the cartesian grid is simply obtained by taking the average of the traces in the four neighboring elements.

Finally, the question of the regularity of the matrix ${}^t\mathbb{B}\mathbb{M}^{-1}\mathbb{B}$ remains. If ${}^t\mathbb{B}\mathbb{M}^{-1}\mathbb{B}\mathbb{J} = 0$, then ${}^t\mathbb{J}{}^t\mathbb{B}\mathbb{M}^{-1}\mathbb{B}\mathbb{J} = 0$, then $\mathbb{B}\mathbb{J} = 0$. By definition of $\mathbb{B}$, this means that for any field $\vec{E}_h$ in $\mathbb{V}_h$, we have $\int_\Gamma \big(\big(A(\vec{E}_h) \times \vec{n}_\Gamma\big) \times \vec{n}_\Gamma \big) \cdot \vec{j} = 0$. Since the projection A is clearly surjective from $\mathbb{V}_h$ onto $\mathbb{A}_h$, this means that $\int_\Gamma \big(\big(\vec{X}_h \times \vec{n}_\Gamma\big) \times \vec{n}_\Gamma \big) \cdot \vec{j} = 0$ for any $\vec{X}_h$ in $\mathbb{A}_h$. Thus $\vec{j} = 0$ and the matrix is regular as long as it is the case for the standard FDTD-fictitious domain method (which is the case under the compatibility condition on the mesh sizes h and h').

4.3 Summary of the DGTD fictitious domain method

The algorithm proposed is then the following: starting from known fields $\mathbb{E}^n$ and $\mathbb{H}^{n+1/2}$,

1. compute the prediction $\tilde{\mathbb{E}}^{n+1}$ using the DGTD method with no object boundary;
2. project $\tilde{\mathbb{E}}^{n+1}$ onto $\mathbb{A}_h$: for any edge, take the average of the four traces of $\tilde{\mathbb{E}}^{n+1}$ around the edge;
3. compute $\mathbb{J}^{n+1/2}$ as for the classical fictitious domain;
4. correct the electric field $\tilde{\mathbb{E}}^{n+1}$ to obtain $\mathbb{E}^{n+1}$;
5. compute $\mathbb{H}^{n+3/2}$ using the DGTD method with no object boundary.

The algorithm is very simple and the software developed can simply recycle a DGTD method in free space and a fictitious domain method developed for the FDTD [15].

5 Preliminary numerical results

Numerical assessment on a tilted metallic plane. We consider a finite metallic plane illuminated by a dipole and test the scattered field computed with or without the fictitious domain approach, if the plane is tilted or not. The 1.5m × 1.5m × 1.5m computational domain is centered on the dipole (Gaussian excitation with central frequency 1 GHz). The 0.6m × 0.6m metallic plane is located at a distance of 0.375 m from the dipole. The $100 \times 100 \times 100$ volumic grid has a grid size of $h_V = 15\ mm$ and the surfacic mesh is made of 1000 edges (lengths in the range $[30\ mm; 43\ mm]$). The frequency response at f =1 GHz is computed for four different configurations. In the first two configurations, the plane is not tilted. It

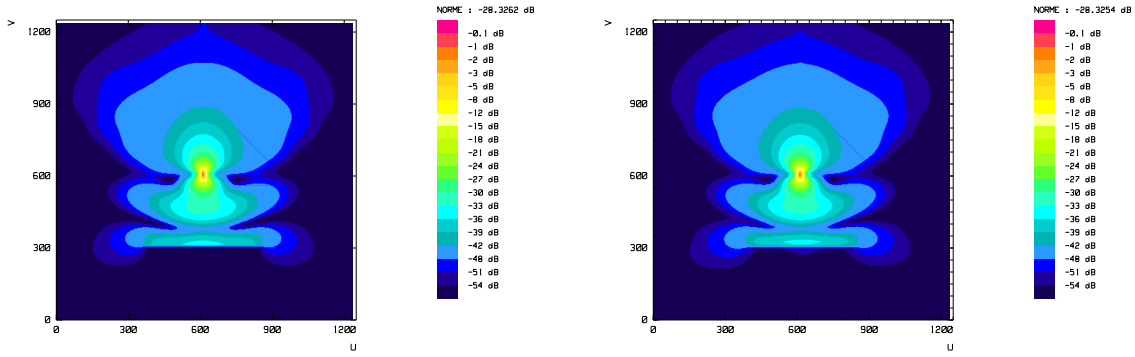

Figure 11: Contours (in a cut) for the electric field at f =1 GHz with untilted plane: A) standard boundary (left) and B) fictitious domain approach (right).

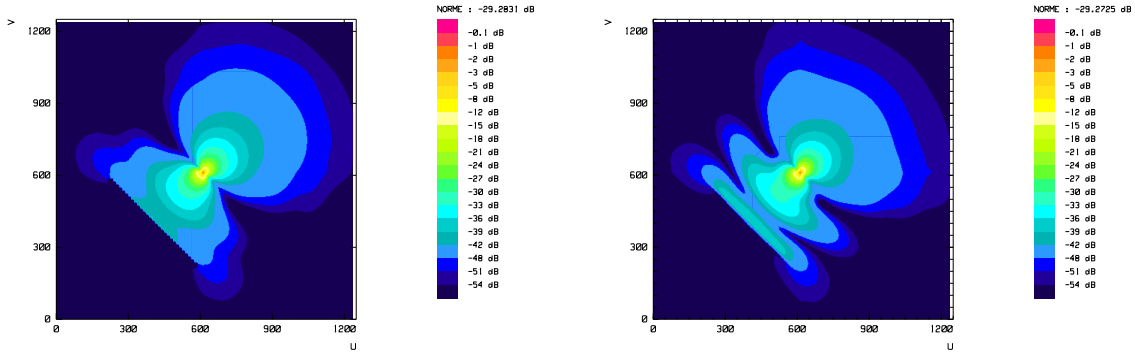

Figure 12: Contours (in a cut) for the electric field at f =1 GHz with untilted plane: C) standard staircased boundary (left) and D) fictitious domain approach (right).

is exactly located on element interfaces and taken into account either A) classically (standard weak treatment of a metallic boundary condition) or B) with the fictitious domain approach. Electric field contour plots for both cases on Figure 11 show a very good agreement. In the last two configurations, the plane is actually tilted. It is taken into account either C) classically with an approximate staircased metallic boundary or D) with the fictitious domain approach. Electric field contour plots for both cases are shown on Figure 12. The contours obtained in case D) are in very good agreement with those of cases A) and B). The contours obtained with the staircased boundary differ significantly.

Scattering by a metallic sphere. We assess here the ability of the method to handle curved surfaces. We consider the scattering by a metallic sphere (radius 0.5 m) of the field generated by a dipole (modulated Gaussian signal with central frequency f =0.5 GHz). The dipole is located 0.385 m away from the sphere. The 108×120×108 volumic mesh is such that h = 15 mm and the unstructured triangular surfacic mesh of the sphere is quite regular, with 10248 edges (lengths in the range $[18\ mm; 23\ mm]$). Contours of the electric field at frequency f =0.5 GHz are shown on Figure 13 in a cut plane enclosing the dipole and the center of the sphere. The sphere is quite accurately taken into account. However, some part of the field is transmitted inside the sphere, which is usual with fictitious domain methods (as the metallic boundary condition is satisfied in a "least-square sense" only). In the present case, the attenuation of the field through the sphere is approximately 40 dB.

Cylinder horn antenna with no local refinement. We consider a revolution horn antenna whose geometry is sketched on Figure 14 along with a view of the surfacic triangulation used. The geometry considered here would lead to the generation of a complex volumic finite element mesh around the structure or a

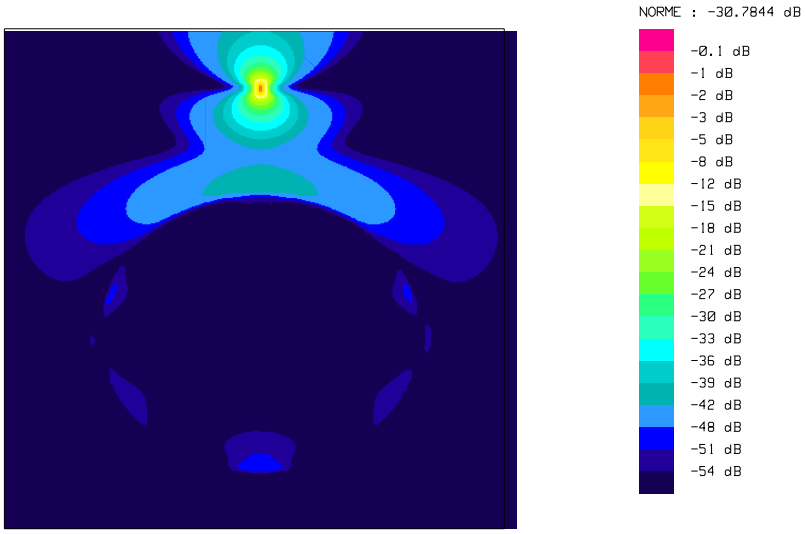

Figure 13: Electric field at frequency f =0.5 GHz.

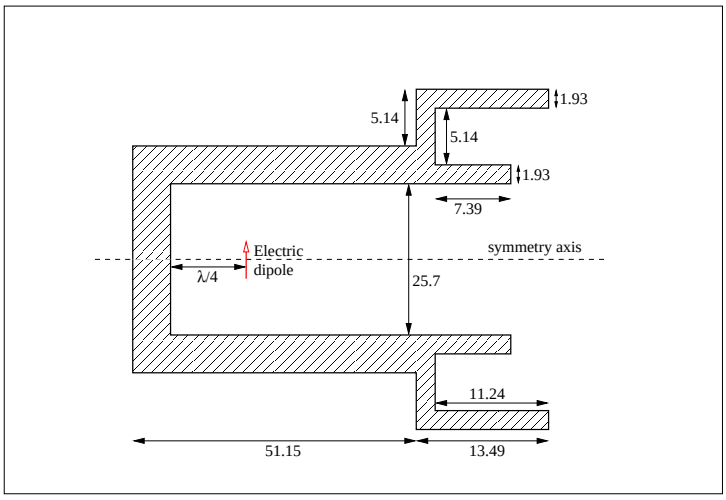

Figure 14: Cylinder horn antenna fed by an electric dipole located at $\lambda_g/4$ (for $f = 7.5$ GHz) inside the cylinder waveguide (lengths in mm).

very fine uniform cartesian grid in case a FDTD is used. Therefore, it is particularly well fitted to the use of a fictitious domain technique. However, the fine ridges (1.93 mm) require the use of a very fine surfacic mesh, typically in $\lambda/20$, as the first two modes of the horn are the TE_{11} mode (with frequency 7.056 GHz) and the TM_{01} mode (with frequency 8.929 GHz) and the horn is excited by an electric dipole with central frequency f_0 =7.5 GHz. We have used a 3492-edge surfacic mesh (edge lengths between 1.93 mm and 7.39 mm (see Figure 15). For the time-domain computation, a uniform volumic mesh with $h = 1\ mm \sim \lambda/40$ and with $60 \times 84 \times 61$ elements was used. Frequency planar cuts at f_0 =7.5 GHz after 4000 time-steps of $\Delta t = 1.9\ 10^{-12} s$ are shown on Figure 16. The cylindrical geometry of the dipole is quite well taken into account. The horn antenna scatters in the axis direction. Also, a low field intensity is artificially scattered through the metallic walls of the antenna.

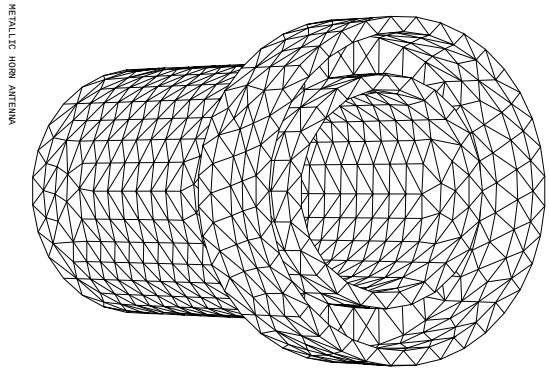

Figure 15: Surfacic mesh of the cylinder horn antenna.

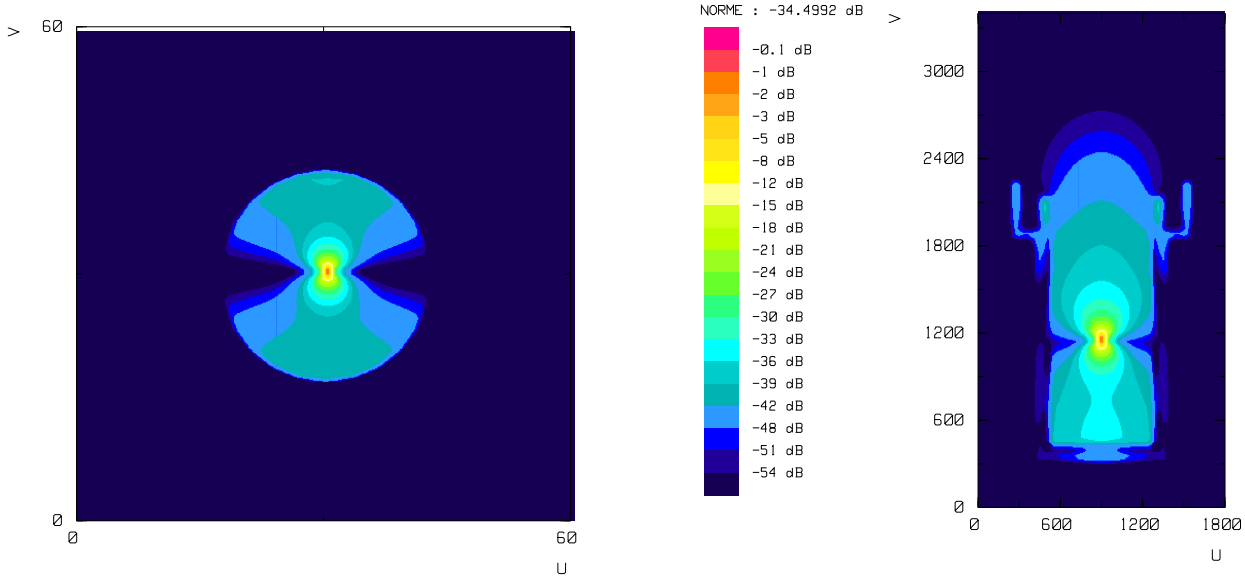

Figure 16: Frequency planar cuts (at the dipole location) of the electric field at 7.5 GHz: normal plane (left), axial plane (right).

Helix antenna with local refinement. We consider the symmetric helix antenna represented on top part of Figure 17. The tiny diameter of the helical wire leads to surfacic meshes with some element edges being very small compared to the total length of the structure, and therefore to huge volumic meshes if not locally refined. We used a 5648-element triangular surfacic mesh of the wire, with edge lengths in the range $0.296 - 0.5\ mm$ (see bottom part of Figure 17). For the volumic mesh, in order to verify the surfacic/volumic meshes compatibility condition, we have taken $h_V = 0.148\ mm$. A uniform mesh of the $20\ mm \times 20\ mm \times 65\ mm$ computational domain would lead to more than 8 million elements. In order to reduce the number of elements, each helix is framed inside a $6\ mm \times 6\ mm \times 26\ mm$ box. Outside of the box, the mesh is de-refined with a ratio equal to 4. This leads to a locally refined mesh with approximately 680k elements.

The double helix antenna is excited by an electric dipole located at the center, with central frequency 13 GHz. After 5000 times steps of $\Delta t \sim 1.14\ 10^{-13} s$, frequency fields at 13 GHz are computed. A contour plot of the electric field (cut in an axial plane) is shown on Figure 18. The contours show the geometry

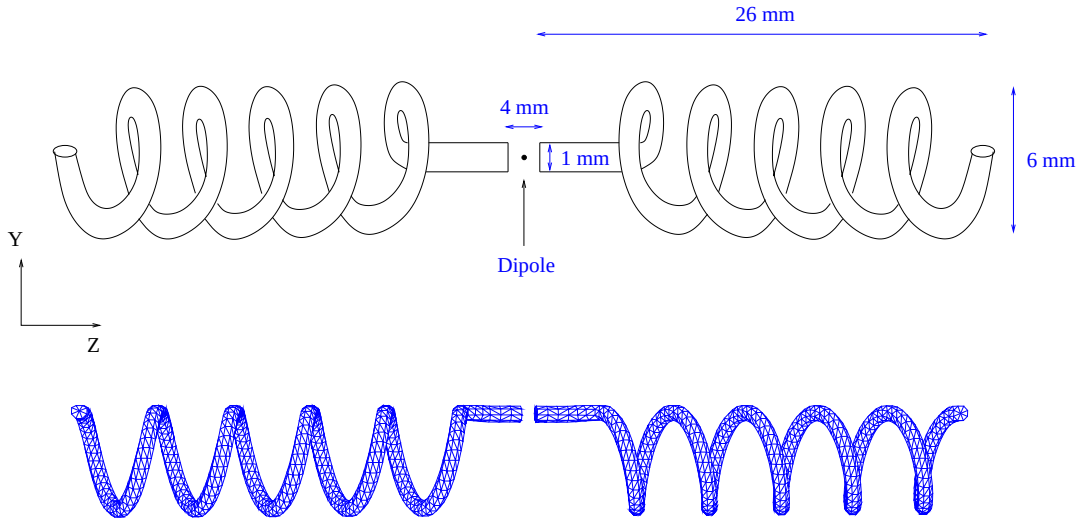

Figure 17: Symmetric helix antenna (top) with the surfacic mesh used (bottom).

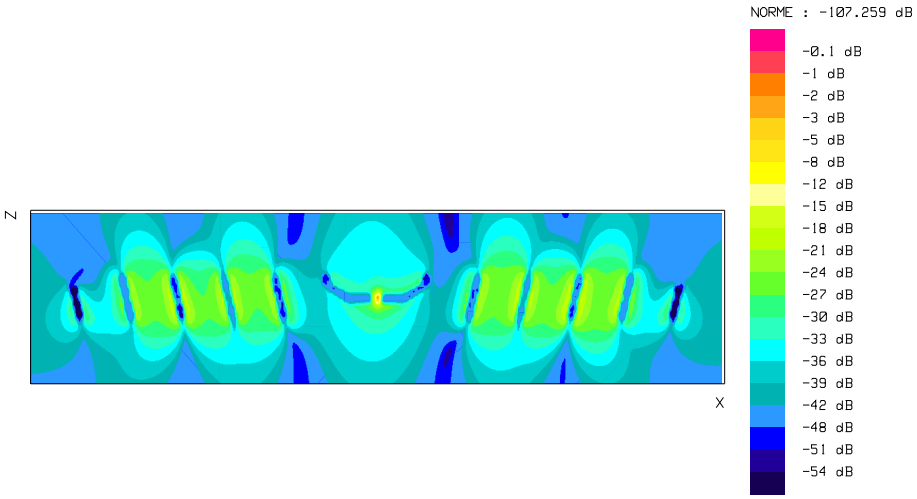

Figure 18: Frequency cut in an axial plane) of the electric field.

has been taken into account. Intensive numerical tests should now investigate the accuracy of such computations.

6 Conclusion

We have proposed in this paper an explicit DGTD method dealing with locally-refined block-Cartesian grids, based on orthogonal brick elements. The method, which is a particular instance of DGTD non-diffusive methods with centered numerical fluxes and a leap-frog time-scheme, can be coupled with a fictitious domain approach in order to handle efficiently perfectly conducting structures with complex geometries, including very small geometrical details. Preliminary and promising numerical results on realistic industrial configurations have been presented.

Some further work is required, in particular in the actual use of the method on existing industrial

configurations. At the same time, a theoretical work is still ahead to prove the convergence of the method, the construction of such a proof could also give insights for a more accurate treatment of the fictitious boundary condition that could be set on the magnetic field.

Acknowledgments

The authors thank P. Brachat et P. Ratajczak of France Telecom R& D for their constant help and S. Lanteri of INRIA for fruitful discussions and kind hosting in his research team.

References

[1] S. Abarbanel and Gottlieb. A mathematical analysis of the pml method. *J. Comput. Phys.*, 134:357–363, 1997.

[2] M. Ainsworth. Dispersive and dissipative behaviour of high order discontinuous Galerkin finite element methods. *J. Comput. Phys.*, 198:106–130, 2004.

[3] I. Babuska. The finite element method with lagrange multipliers. *Soviet. J. Numer. Anal. Math. Modelling*, 20:179–192, 1973.

[4] E. Bécache and P. Joly. On the analysis of berenger's perfectly matched layers for maxwell's equations. *M2AN*, 1,36:87–120, 2002.

[5] J.P. Bérenger. Three-dimensional perfectly matched layer for the absorption of electromagnetic waves. *Journal of Computational Physics*, 127:363–379, 1996.

[6] A. Bouquet. *Caractérisation de structures rayonnantes par une méthode de type Galerkin Discontinu associée à une technique de domaines fictifs.* PhD thesis, Université de Nice - Sophia Antipolis, décembre 2007.

[7] A.C. Cangellaris and D.B. Wright. Analysis of the numerical error caused by the stair-stepped approximation of a conducting boundary in fdtd simulations of electromagnetic phenomena. *IEEE Transaction on Antennas and propagation*, 39(10):1518–1525, 1991.

[8] N. Canouet, L. Fezoui, and S. Piperno. Discontinuous Galerkin Time-Domain solution of Maxwell's equations on locally-refined nonconforming cartesian grids. *COMPEL*, 24(4):1381–1401, 2005.

[9] J.-P. Cioni, L. Fezoui, L. Anne, and F. Poupaud. A parallel FVTD Maxwell solver using 3D unstructured meshes. In *13th annual review of progress in applied computational electromagnetics*, pages 359–365, Monterey, California, 1997.

[10] B. Cockburn, G. E. Karniadakis, and C.-W. Shu, editors. *Discontinuous Galerkin methods. Theory, computation and applications.*, volume 11 of *Lecture Notes in Computational Science and Engineering*. Springer-Verlag, Berlin, 2000.

[11] F. Collino, P. Joly, and F. Millot. Fictitious domain method for unsteady problems: Application to electromagnetic scattering. *J. Comput. Phys.*, 138:907–938, 1997.

[12] F. Collino and C. Tsogka. Application of the pml absorbing layer model to the linear elastodynamic problem in anisotropic heteregeneous media. *Geophysics*, 66,1:294–307, 2001.

[13] B. Engquist and A. Madja. Absorbing-boundary conditions for the numerical simulation of waves. *Mathematics of computation*, 31:629–651, 1977.

[14] L. Fezoui, S. Lanteri, S. Lohrengel, and S. Piperno. Convergence and stability of a Discontinouous Galerkin time-method for the 3D heterogeneous Maxwell equations on unstructured meshes. *ESAIM: M2AN*, 39, n6:1149–1176, 2005.

[15] S. Garcés. *Application des méthodes de domaines fictifs à la modélisation de structures rayonnantes tridimensionnelles*. PhD thesis, ENSAE, 1998.

[16] R. Glowinski and Y. Kuznetsov. On the solution of the dirichlet problem for linear elliptic operators by a distribued lagrange multiplier method. *C. R. Acad. Sci Paris*, t. 327, Serie I:693–698, 1998.

[17] R. Glowinski, T. Pan, and J.Periaux. A fictitious domain method for dirichlet problem and applications. *Computer Methods in Applied Mechanics and Engineering*, 11:283–303, 1994.

[18] G.Mur. Absorbing boundary conditions for the finite difference approximation for the time domain electromagnetic field equations. *IEEE Transactions on Electromagnetic Compatibility*, EMC-23, n4:317–382, 1981.

[19] Guo-Chunling, Yao-Wuliev, and K.K. Mei. Full-wave analysis of coplanar waveguide and slot line using the time-domain finite-difference method. *IEEE Transactions on MTT*, 37, n12, dec. 1989.

[20] J.S. Hesthaven and T. Warburton. Nodal high-order methods on unstructured grids. I: Time-domain solution of Maxwell's equations. *J. Comput. Phys.*, 181(1):186–221, 2002.

[21] Ansoft HFSS, 3D Full-wave Electromagnetic Field Simulation, http://www.ansoft.com/products/hf/hfss/.

[22] R. Holland, V. P. Cable, and L. C. Wilson. Finite-volume time-domain (FVTD) techniques for EM scattering. *IEEE Trans. Electromagn. Compat.*, 33(4):281–294, 1991.

[23] F. Q. Hu. On absorbing boundary conditions for linearized euler equations by a perfectly matched layer. *J. Comp. Phys.*, 129:201, 1996.

[24] P. Joly and C. Poirier. A new second order 3D edge element on tetrahedra for time dependent Maxwell's equations. In A. Bermudez, D. Gomez, C. Hazard, P. Joly, and J.-E. Roberts, editors, *Fifth International Conference on Mathematical and Numerical Aspects of Wave Propagation*, pages 842–847, Santiago de Compostella, Spain, July 10-14 2000. SIAM.

[25] I.S. Kim and W.J.R. Hoefer. A local mesh refinement alogoritm for the fd-td method to solve maxwell's equations. *IEEE Trans. Microwave Theory Tech.*, 38(6):812–815, June 1990.

[26] J.-F. Lee and Z. Sacks. Whitney elements time domain (WETD) methods. *IEEE Trans. Magn.*, 31(3):1325–1329, 1995.

[27] J.-C. Nédélec. Mixed finite elements in $\mathbb{R}^3$. *Numer. Math.*, 35:315–341, 1980.

[28] P.G. Petropoulos. Reflectionless sponge layers as absorbing condition for the numerical solution of maxwell's equations in rectangular, cylindrical, and spherical coordinates. *SIAM J. Appl. Math.*, 60:1037–1058, 2000.

[29] S. Piperno. Symplectic local time-stepping in non-dissipative DGTD methods applied to wave propagation problems. *ESAIM: M2AN*, 40, n5:815–841, 2006.

[30] S. Piperno, M. Remaki, and L. Fezoui. A non-diffusive finite volume scheme for the 3D Maxwell equations on unstructured meshes. *SIAM J. Numer. Anal.*, 39(6):2089–2108, 2002.

[31] D.T. Prescott and N.V. Shuley. A method for incorporating different sizes cells into the fd-td analysis technique. *IEEE Microwave Guided Wave Lett.*, 2:434–436, 1992.

[32] R.Garg and K.C. Gupta. Expressions for wavelengh and impedance of a slotline. *IEEE Transactions on MTT*, MTT-24:523, Aug. 1976.

[33] S.Wam, Haoling, and Tatsuo Itoh. Characterisation of uniform microstrip line and its discontinuities using the time-domain method of lines. *IEEE Transactions on MTT*, 37, n12, dec. 1989.

[34] E. Turkel and A. Yefet. Absorbing pml boundary layers for wave-like equations. *Applied Numerical Mathematics*, 27:533–557, 1998.

[35] V.Girault and R. Glowinski. Error analysis of a fictitious domain method applied to a dirichlet problem. *Jap. J. Ind. Appli. Math.*, 12:487–514, 1995.

[36] K. S. Yee. Numerical solution of initial boundary value problems involving Maxwell's equations in isotropic media. *IEEE Trans. Antennas and Propagation*, AP-16:302–307, 1966.

[37] L. Zhao and A. C. Cangellaris. A general approach for the development of unsplit-field time-domain implementations of perfectly matched layers for fdtd grid truncation. *IEEE Microwave and Guided Letters*, 6,5, 1996.